Nonlinear Polariton Fluids in a Flatband Reveal Discrete Gap Solitons

V. Goblot, B. Rauer, F. Vicentini, A. Le Boité, E. Galopin, A. Lemaître, L. Le Gratiet, A. Harouri, I. Sagnes, S. Ravets, et al.

Nonlinear Polariton Fluids in a Flatband Reveal Discrete Gap Solitons

V. Goblot,[1,*] B. Rauer,[1,2] F. Vicentini,[3] A. Le Boité,[3] E. Galopin,[1] A. Lemaître,[1] L. Le Gratiet,[1] A. Harouri,[1] I. Sagnes,[1] S. Ravets,[1] C. Ciuti,[3] A. Amo,[4] and J. Bloch[1]

[1]*Centre de Nanosciences et de Nanotechnologies (C2N), CNRS, Université Paris-Sud, Université Paris-Saclay, 91120 Palaiseau, France*

[2]*Vienna Center for Quantum Science and Technology, Atominstitut, TU Wien, Stadionallee 2, 1020 Vienna, Austria*

[3]*Université de Paris, Laboratoire Matériaux et Phénomènes Quantiques, CNRS, F-75013 Paris, France*

[4]*Université de Lille, CNRS, UMR 8523 -PhLAM- Physique des Lasers Atomes et Molécules, F-59000 Lille, France*

(Received 7 May 2019; revised manuscript received 26 July 2019; published 13 September 2019)

Phase frustration in periodic lattices is responsible for the formation of dispersionless flatbands. The absence of any kinetic energy scale makes flatband physics critically sensitive to perturbations and interactions. We report on the experimental investigation of the nonlinear response of cavity polaritons in the gapped flatband of a one-dimensional Lieb lattice. We observe the formation of gap solitons with quantized size and abrupt edges, a signature of the frozen propagation of switching fronts. This type of gap soliton belongs to the class of truncated Bloch waves, and has only been observed in closed systems up to now. Here, the driven-dissipative character of the system gives rise to a complex multistability of the flatband nonlinear domains. These results open up an interesting perspective regarding more complex 2D lattices and the generation of correlated photon phases.

DOI: 10.1103/PhysRevLett.123.113901

Geometric frustration in periodic quantum media is responsible for the existence of energy bands with no dispersion. These systems are extremely sensitive to any perturbation like disorder or interaction. Fascinating many-body physics occurs in flatbands, among which are the formation of spin liquids and spin ices [1], itinerant ferromagnetism [2,3], fractional quantum Hall states [4], or superconductivity in twisted bilayer graphene [5,6]. In the quest for emulation of this rich phenomenology in controlled systems, pioneering works on frustrated lattices with a flatband have been realized in recent years [7], using different analog systems like cold atoms [8,9], arrays of coupled optical waveguides [10–12], or semiconductor microcavities [13–17]. However, most of these works have been limited so far to the linear regime, where particle-particle interactions are negligible. Despite interesting theoretical predictions [18,19], the experimental exploration of many-body physics in synthetic frustrated flatbands remains in its infancy.

Exciton polaritons in semiconductor microcavities have emerged as a powerful platform to study quantum fluids in a driven-dissipative context [20]. Polaritons are quasiparticles arising from the strong radiative coupling between photons confined in a semiconductor microcavity and excitons confined in quantum wells (QWs). Their excitonic component provides significant repulsive interactions (equivalent to a Kerr-like nonlinearity), and the dissipative nature of the system allows for direct injection of polaritons at a given energy. This has enabled the observation of hydrodynamic features including superfluidity [21], nucleation of vortices [22,23], and solitons [24,25]. Additionally, the potential landscape probed by polaritons can be sculpted using a variety of techniques [26]. This allows controlling the polariton band structure by engineering lattices and offers a versatile playground to investigate the interplay between kinetic and interaction energy. Recently, several groups have reported the realization of a flatband for polaritons: fragmentation of a polariton condensate induced by disorder was observed [15], as well as interesting polarization textures induced by spin-orbit coupling [17].

In this Letter, we report the experimental investigation of the nonlinear response of polaritons in the flatband of a one-dimensional Lieb lattice of coupled micropillar cavities. We observe the generation of bright quantized nonlinear domains with abrupt and well-defined edges. These sharp profiles are due to the fact that the interaction energy induced by the drive cannot be accommodated as kinetic energy in the flatband. As a result, propagation of switching fronts is frozen. The size of the domains evolves through abrupt jumps as the pumping power is swept, and multistability is evidenced around each of these jumps. Theoretical analysis of the observed features indicates that these domains belong to the family of gap solitons named truncated Bloch waves [27–31], which had never been observed in a driven-dissipative context.

The 1D Lieb lattice [see Fig. 1(a)] is one of the simplest lattices hosting a flat energy band [2]. The unit cell (UC) contains three—A, B, C—sites linked by nearest-neighbor couplings t (t') between B and C (A and B) sites. In the

tight-binding approximation, the corresponding single-particle Hamiltonian is

$$\hat{H} = \sum_{l,n} E_l |l_n\rangle\langle l_n| - \sum_n [t(|B_n\rangle\langle C_n| + |B_n\rangle\langle C_{n+1}|) + t'|A_n\rangle\langle B_n| + \text{H.c.}], \quad (1)$$

where $|l_n\rangle$, with $l \in \{A, B, C\}$, is the state on site l in the nth unit cell, with on-site energy E_l. The energy spectrum of the 1D Lieb lattice presents three bands. While eigenfunctions in the lower (upper) band are constructed with the same (opposite) phase for neighboring sites, eigenfunctions for the middle band show alternating phase sign on the A, C sublattice. This creates a phase frustration on sites B: when $E_A = E_C$, a destructive interference induces zero wave function amplitude on B sites. As a result, the middle band is flat with localized eigenstates of the form $|f_n\rangle = (|A_{n-1}\rangle - |C_n\rangle + |A_n\rangle)/\sqrt{3}$, as shown in Fig. 1(a). When $E_A \neq E_C$, the interference on B sites is not fully destructive and the middle band becomes dispersive.

To experimentally implement a polariton Lieb lattice, we use a semiconductor heterostructure grown by molecular beam epitaxy. It consists of a λ GaAs layer embedded between two $Ga_{0.9}Al_{0.1}As/Ga_{0.05}Al_{0.95}As$ distributed Bragg reflectors (DBRs) with 36 (top) and 40 (bottom) pairs (quality factor $Q \approx 50000$). A single 8 nm $In_{0.05}Ga_{0.95}As$ QW is inserted at the center of the cavity, resulting in a 3.5 meV Rabi splitting. The cavity is processed into an array of coupled micropillars [Fig. 1(b)] using electron beam lithography and dry etching down to the GaAs substrate. Each micropillar is mapped to a site of the tight-binding Hamiltonian while the coupling between sites is provided by the finite overlap between neighboring pillars. The on-site energy of the lowest-energy mode in each micropillar is controlled by the pillar diameter, but also depends on the number of adjacent pillars, whose proximity reduces the local confinement. Thus a fine-tuning in the pillar diameters is required to match A and C on-site energies and obtain a flatband. We choose a 2.4 μm distance between adjacent pillars (resulting in UC size $a = 4.8$ μm), and 3.0, 2.8, and 2.9 μm for the diameters of A, B, and C pillars, respectively.

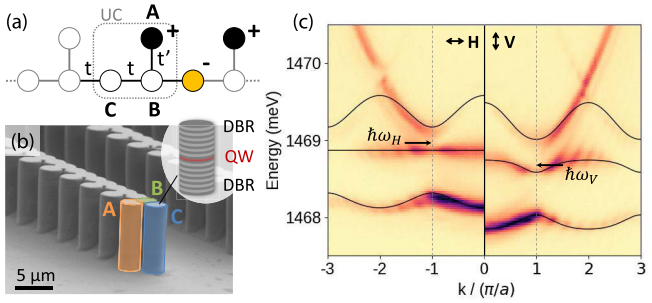

FIG. 1. (a) Schematic representation of the 1D Lieb lattice. Filled circles: localized eigenstate with relative phase indicated with signs. (b) Scanning electron microscopy image of a micropillar lattice. Inset: Schematic representation of a single pillar with embedded layers. (c) Energy resolved photoluminescence measured in momentum space under nonresonant pumping, for linear polarization parallel (H) and orthogonal (V) to the lattice. Solid lines: calculated dispersion solving a tight-binding Hamiltonian. For H polarization, $E_A = E_C = 1468.9$ meV, $E_B = E_C - 0.30$ meV, and $t = t' = 0.30$ meV; for V polarization, $E_A = E_C + 0.18$ meV, $E_B = E_C - 0.30$ meV, and $E_C = 1468.6$ meV, with the same t, t'. Arrows indicate the energy $\hbar\omega_{H,V}$ and wave vector of the resonant pump.

Optical spectroscopy is performed at 4 K, using a tunable continuous wave (cw) monomode excitation laser focused on the 1D lattice. The signal is collected in transmission geometry through the back of the sample, using a lens with 0.5 numerical aperture, and focused on the entrance slit of a spectrometer coupled to a CCD camera. The emission is analyzed in real or momentum space, by imaging either the sample surface or the Fourier plane of the collection lens. Using a $\lambda/2$ wave plate and a polarizer, we select the linearly polarized emission either parallel (H) or orthogonal (V) to the lattice.

First, we characterize the band structure of the polariton lattice in the linear regime. The lattice is excited nonresonantly tuning the laser energy around 1.6 eV, with a Gaussian-shaped elongated spot and weak pumping power. The energy difference between the uncoupled cavity mode and the exciton resonance amounts to -3.5 meV. The momentum-space resolved emission for both H and V polarization is shown in Fig. 1(c). Three bands are evidenced arising from hybridization of micropillar confined modes. They are well reproduced by tight-binding calculations, except for the upper band where the expected band folding is not observed in the experiment. This deviation can be explained in terms of mixing with higher-energy bands, neglected by the tight-binding description. For H polarization, the middle band is dispersionless and is gapped from the two other bands. Because of polarization dependent boundary conditions for the electromagnetic field, the flatband condition cannot be achieved simultaneously for two orthogonal linear polarizations [15]. Indeed, under V polarization all bands are dispersive. The faint intensity modulation visible in Fig. 1(c) arises from multiple reflections between the bottom mirror and the polished back side of the substrate.

To investigate the polariton nonlinear response in the flatband, we inject polaritons with a quasi-resonant laser at energy detuning Δ from the flatband. In the experiments described in the following, the flatband is at energy $E_C = 1468.9$ meV and the laser energy $\hbar\omega_H$ is blueshifted by $\Delta = 90$ μeV, corresponding to about one-third of the energy gap separating the flatband from the upper one [Fig. 1(c)]. The pumping beam is polarized along H and focused into a Gaussian-shaped elongated spot of 40×3 μm^2 FWHM [Fig. 2(c)]. Its 5.0° angle of incidence matches the edge

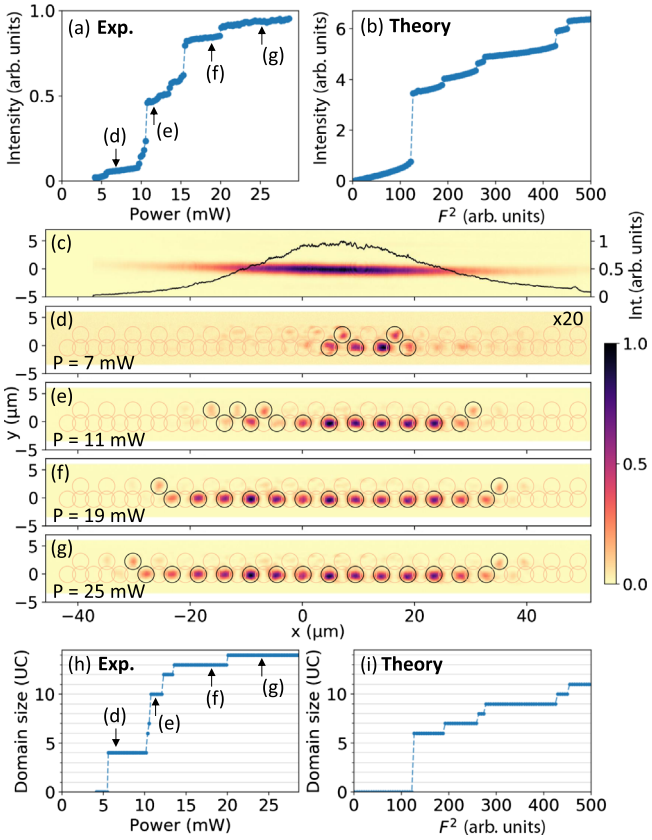

FIG. 2. (a),(b) Total emission intensity (a) measured and (b) calculated under resonant excitation tuned to energy $\hbar\omega_H$ as a function of power. (c) 2D real-space image of the excitation spot. Black line: spatial profile integrated over the transverse direction. (d)–(g) Real-space emission intensity measured at pumping powers indicated in (a). Highly excited micropillars are indicated by circles. (h),(i) Size of the nonlinear domains (h) measured and (i) calculated as a function of (h) excitation power, (i) F^2.

of the first Brillouin zone (BZ), i.e., $k = \pi/a$, enabling efficient coupling to the flatband modes [32].

Figure 2(a) presents the measured total emitted intensity when increasing the excitation power P. Several abrupt jumps are observed separated by plateaus where the intensity weakly varies. To discuss the origin of the observed features, we show in Figs. 2(d)–2(g) spatial emission patterns measured for different excitation powers. For $P = 7$ mW, above the lowest power intensity jump, Fig. 2(d) evidences the formation of a 4 UC nonlinear domain. It is located around the center of the excitation spot and its shape does not evolve when P is further increased, up to a power of 10 mW, where the next jump happens. We then observe the formation of a larger nonlinear domain with 10 UCs. Actually, every jump corresponds to an evolution of the domain size by a discrete number of UCs, as summarized in Fig. 2(h). The size of the domains is well defined because their edges are extremely sharp: the emission intensity drops by more than an order of magnitude over one UC on each side.

To get more insight into the physics, we solve the steady state of a discretized Gross-Pitaevskii equation that includes pump and loss terms [34]. The evolution of the polariton amplitude ψ_n on site n, under a cw resonant drive, is governed, in the frame rotating at the drive frequency ω, by the equation

$$i\hbar\frac{d\psi_n(t)}{dt} = \left(E_n - \hbar\omega + \hbar g|\psi_n(t)|^2 - i\frac{\gamma}{2}\right)\psi_n(t) - \sum_m t_{nm}\psi_m(t) + iFe^{-x_n^2/4\sigma^2}e^{-ik_p x_n}, \quad (2)$$

where $\hbar g$ is the polariton-polariton interaction constant and γ is the polariton linewidth. E_n is the on-site energy and t_{nm} are the couplings to neighboring sites, deduced from t and t' defined before [32]. F is the drive amplitude, $k_p = \pi/a$ the mean wave vector of the drive, and x_n the spatial position of site n. The spatial distribution of the drive excitation is chosen Gaussian with $\sigma = 3.5$ UCs and its detuning from the flatband, defined as $\Delta = \hbar\omega - E_C$, is $\Delta = 3\gamma = 90$ μeV.

Figure 2(b) presents the calculated total intensity in a 40 UC chain when increasing the drive amplitude. A series of abrupt jumps is observed in good qualitative agreement with the experiment. Similar to the experiment, the simulated steady-state spatial profiles consist in nonlinear domains of finite size [32], and each jump in the total intensity corresponds to a discrete change in the domain size.

The origin of these quantized nonlinear domains in the flatband is intimately linked to the fact that the pump energy lies in an energy gap. Locally, the system switches into the nonlinear regime (with high polariton intensity) when the local pump intensity is higher than a threshold value, so that the local interaction energy $\hbar g|\psi|^2 \gtrsim \Delta$. Outside this high excitation region, the system remains in the linear regime with very low intensity because the excitation laser lies within an energy gap. This is the reason why abrupt edges are formed. The size of the domain is determined by the number of UCs for which the local pump intensity is higher than the threshold value. Because of the Gaussian shape of the excitation spot, the threshold condition is reached for more and more UCs as the power is increased, and domains of increasing size are formed. If the excitation profile was completely flat, all excited UCs would switch simultaneously.

These nonlinear states belong to the general family of gap solitons. They have been discussed in a different context [27,28] and named truncated Bloch waves (TBWs), because their pattern is similar to a spatial portion of the excited Bloch states. Notice that in our system, TBWs can also be observed when exciting in a gap above a dispersive band, as illustrated by simulations presented in the Supplemental Material [32]. In a flatband, there is no kinetic energy to overcome so that discrete TBWs are

formed as soon as the laser detuning overcomes the band linewidth.

A significant difference between numerical simulations and experiments is revealed in the quantitative domain size versus F. Once the first domain is formed (at $F^2 = 120$), the calculated domain size increases by exactly one UC at each jump [see Fig. 2(i)]. The situation is different in the experiment where, for instance, an increase of 6 UCs is observed at 10 mW [Fig. 2(h)]. In the Supplemental Material [32], we show that disorder in the on-site energies explains this apparent discrepancy. Experimentally, disorder mainly stems from small fluctuations in the pillar size and shape, caused by etching. A local redshift of the flatband eigenstates acts as a barrier for the nonlinear domain: when the excitation strength is sufficient to overcome this barrier, the domain size can abruptly increase by several unit cells, as observed experimentally. Notice also that the drive with the wave vector at the edge of the BZ imposes a π phase difference between adjacent UCs. This creates destructive interference on A sites explaining why A sites are generally dark within the nonlinear domains. Bright A sites are only observed at the edges of the nonlinear domains or in regions where disorder is of the order of the interaction energy, thus altering the interference [see, for instance, Figs. 2(d) and 2(e), left-hand side].

TBWs have been experimentally observed in closed systems [29–31], but to our knowledge have never been reported in a driven-dissipative system. Associated to the presence of dissipation, such nonlinear photonic systems are expected to present hysteretic behaviors [20,35]. To probe this property, we excite the flatband with $\Delta = 90$ μeV and scan the power up and down around each nonlinear jump of the intensity. This reveals multiple hysteresis cycles, summarized in Fig. 3(a). In fact, each abrupt jump is associated with a hysteresis cycle. Depending on the value of the power and the power ramp history, several configurations of nonlinear domains can be achieved. As an illustration, Figs. 3(b)–3(e) show four nonlinear spatial patterns which can be generated for $P = 10.2$ mW. Each of them shows a TBW soliton, with a well-defined number of bright unit cells and no emission outside the nonlinear domains. Thus the polariton nonlinear response of the flatband reveals complex multistable behavior when scanning the power up and down.

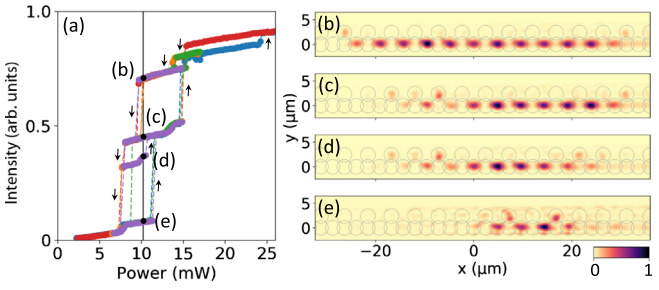

FIG. 3. Total intensity measured under resonant excitation of the flatband (same excitation parameters as in Fig. 2) when scanning the excitation power up and down as indicated by arrows. (b)–(e) Real-space emission patterns measured for $P = 10.2$ mW on different branches as indicated in (a).

We now compare the experiments described above with the nonlinear response when pumping the system within a dispersive band. Direct comparison can be done in the very same lattice simply by injecting polaritons with an excitation linearly polarized along the V direction. The polarization dependent on-site energies result in a middle band that is dispersive in this case [Fig. 1(c), right-hand panel]. We use pumping conditions comparable to those used in Fig. 2: $\Delta = 60$ μeV with respect to the bottom of the band, and the same angle of incidence [Fig. 1(c)]. The results are presented in Fig. 4(a): a nonlinear increase in the total emitted intensity is observed at $P = 10$ mW, followed by an abrupt intensity jump at $P = 17$ mW, associated with a hysteresis cycle. The emission spatial pattern measured in the nonlinear regime for $P = 19$ mW is shown in logarithmic scale in Fig. 4(c). Polariton propagation out of the

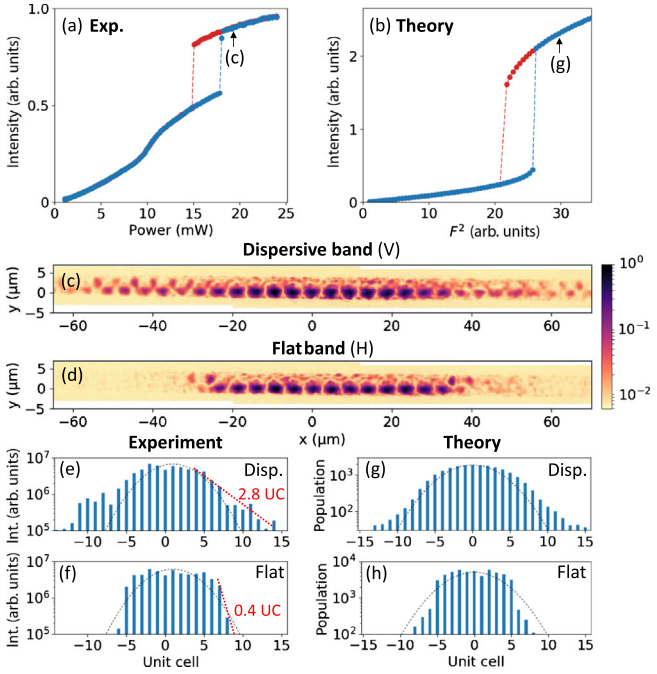

FIG. 4. (a) Total intensity measured as a function of excitation power under V polarized excitation tuned to an energy $\hbar\omega_V$. (b) Corresponding calculated intensity as a function of F^2. In (a) and (b), blue (red) color corresponds to increasing (decreasing) excitation power. (c),(d) Spatially resolved emission represented in logarithmic color scale measured for $P = 19$ mW (c) in the dispersive (V polarized pump) and (d) in the flatband (H polarized pump). (e),(f) Measured integrated intensity on C sites extracted from (c),(d). Black lines, pump spot profile; red line, exponential fit of the emission intensity spatial decay. (g),(h) Calculated intensity on C sites for (g) a dispersive band ($E_A = 6\gamma$) and (h) a flatband ($E_A = 0$) considering (g) $\Delta = 3\gamma$, $F^2 = 300$ and (h) $\Delta = 2\gamma$, $F^2 = 30$.

pumping region is clearly evidenced: the emission spreads over the entire portion of the lattice under investigation, in stark contrast with the case of the flatband [also shown in logarithmic scale in Fig. 4(d)]. Exponential fits to the intensity profiles [see Figs. 4(e) and 4(f)] allow us to estimate a polariton propagation distance of 13.6 μm (2.8 UCs) for the dispersive band, to be compared to only 2.1 μm (0.4 UCs) for the flatband. Polariton propagation outside the high density region is possible in the dispersive band thanks to the conversion of interaction energy into kinetic energy. The resulting propagation of switching fronts has been previously used to realize a spin switch [36]. When injecting the quantum fluid into a gap, such propagation is totally suppressed.

We simulated the resonant excitation experiment for the case of the dispersive band. The calculated total intensity shown in Fig. 4(b) presents a single hysteresis cycle, in agreement with previous reports [20,35]. In the Supplemental Material, we show that the first nonlinear increase observed in the experiment at $P = 10$ mW is well accounted for by introducing disorder in the simulation [32]. The spatial profiles calculated for the dispersive and the flatband with parameters corresponding to Figs. 4(e) and 4(f) (no disorder) are shown in Figs. 4(g) and 4(h). They nicely reproduce the difference in intensity profile when propagation of the switching front is frozen (flatband) or not (dispersive band).

In conclusion, we have shown that the nonlinear response of a polariton fluid resonantly injected into a flatband is governed by the emergence of gap solitons of the family of TBWs. They are discrete nonlinear domains whose abrupt edges reflect the freezing of kinetic energy, and show complex multistable patterns under nonhomogeneous spatial excitations. Similar experiments in 2D lattices with geometric frustration, where the flatband is touching a dispersive band (kagome) or crosses Dirac points (2D Lieb lattice), could offer interesting perspectives, as well as the investigation of the Bogoliubov excitations when the flatband is driven in the nonlinear regime. Using polariton structures with stronger interaction strength [37–40], experiments beyond semiclassical approximation could be envisioned: in this context, flatbands are also particularly relevant for the study of many-body correlated phases [41–44].

The authors are grateful to F. Baboux, P. St-Jean, and G. Malpuech for fruitful discussions. This work was supported by the H2020-FETFLAG project PhoQus (Project No. 820392), the QUANTERA project Interpol (ANR-QUAN-0003-05), the French National Research Agency (ANR) project Quantum Fluids of Light (ANR-16-CE30-0021), the Labex NanoSaclay (ICQOQS, Grant No. ANR-10-LABX-0035), the French RENATECH network, the ERC via the Consolidator Grant CORPHO No. 616233, and the Austrian Science Fund (FWF) through the doctoral program CoQuS (W1210) (B. R.), the Labex CEMPI (ANR-11-LABX-0007), the CPER Photonics for Society P4S, the I-Site ULNE (projet NONTOP) and the Métropole Européenne de Lille (project TFlight).

*valentin.goblot@c2n.upsaclay.fr

[1] L. Balents, Nature (London) **464**, 199 (2010).
[2] E. H. Lieb, Phys. Rev. Lett. **62**, 1201 (1989).
[3] H. Tasaki, Phys. Rev. Lett. **69**, 1608 (1992).
[4] D. C. Tsui, H. L. Stormer, and A. C. Gossard, Phys. Rev. Lett. **48**, 1559 (1982).
[5] Y. Cao, V. Fatemi, S. Fang, K. Watanabe, T. Taniguchi, E. Kaxiras, and P. Jarillo-Herrero, Nature (London) **556**, 43 (2018).
[6] Y. Cao, V. Fatemi, A. Demir, S. Fang, S. L. Tomarken, J. Y. Luo, J. D. Sanchez-Yamagishi, K. Watanabe, T. Taniguchi, E. Kaxiras, R. C. Ashoori, and P. Jarillo-Herrero, Nature (London) **556**, 80 (2018).
[7] D. Leykam, A. Andreanov, and S. Flach, Adv. Phys. X **3**, 1473052 (2017).
[8] G.-B. Jo, J. Guzman, C. K. Thomas, P. Hosur, A. Vishwanath, and D. M. Stamper-Kurn, Phys. Rev. Lett. **108**, 045305 (2012).
[9] S. Taie, H. Ozawa, T. Ichinose, T. Nishio, S. Nakajima, and Y. Takahashi, Sci. Adv. **1**, e1500854 (2015).
[10] D. Guzmán-Silva, C. Mejía-Cortés, M. A. Bandres, M. C. Rechtsman, S. Weimann, S. Nolte, M. Segev, A. Szameit, and R. A. Vicencio, New J. Phys. **16**, 063061 (2014).
[11] S. Mukherjee, A. Spracklen, D. Choudhury, N. Goldman, P. Öhberg, E. Andersson, and R. R. Thomson, Phys. Rev. Lett. **114**, 245504 (2015).
[12] R. A. Vicencio, C. Cantillano, L. Morales-Inostroza, B. Real, C. Mejía-Cortés, S. Weimann, A. Szameit, and M. I. Molina, Phys. Rev. Lett. **114**, 245503 (2015).
[13] N. Masumoto, N. Y. Kim, T. Byrnes, K. Kusudo, A. Lffler, S. Höfling, A. Forchel, and Y. Yamamoto, New J. Phys. **14**, 065002 (2012).
[14] T. Jacqmin, I. Carusotto, I. Sagnes, M. Abbarchi, D. D. Solnyshkov, G. Malpuech, E. Galopin, A. Lemaître, J. Bloch, and A. Amo, Phys. Rev. Lett. **112**, 116402 (2014).
[15] F. Baboux, L. Ge, T. Jacqmin, M. Biondi, E. Galopin, A. Lemaître, L. Le Gratiet, I. Sagnes, S. Schmidt, H. E. Türeci, A. Amo, and J. Bloch, Phys. Rev. Lett. **116**, 066402 (2016).
[16] S. Klembt, T. H. Harder, O. A. Egorov, K. Winkler, H. Suchomel, J. Beierlein, M. Emmerling, C. Schneider, and S. Höfling, Appl. Phys. Lett. **111**, 231102 (2017).
[17] C. E. Whittaker, E. Cancellieri, P. M. Walker, D. R. Gulevich, H. Schomerus, D. Vaitiekus, B. Royall, D. M. Whittaker, E. Clarke, I. V. Iorsh, I. A. Shelykh, M. S. Skolnick, and D. N. Krizhanovskii, Phys. Rev. Lett. **120**, 097401 (2018).
[18] R. A. Vicencio and M. Johansson, Phys. Rev. A **87**, 061803(R) (2013).
[19] M. Di Liberto, S. Mukherjee, and N. Goldman, arXiv: 1810.07641.
[20] I. Carusotto and C. Ciuti, Rev. Mod. Phys. **85**, 299 (2013).
[21] A. Amo, J. Lefrère, S. Pigeon, C. Adrados, C. Ciuti, I. Carusotto, R. Houdré, E. Giacobino, and A. Bramati, Nat. Phys. **5**, 805 (2009).

[22] G. Nardin, G. Grosso, Y. Leger, B. Pietka, F. Morier-Genoud, and B. Deveaud-Pledran, Nat. Phys. **7**, 635 (2011).
[23] D. Sanvitto, S. Pigeon, A. Amo, D. Ballarini, M. De Giorgi, I. Carusotto, R. Hivet, F. Pisanello, V. G. Sala, P. S. S. Guimaraes, R. Houdré, E. Giacobino, C. Ciuti, A. Bramati, and G. Gigli, Nat. Photonics **5**, 610 (2011).
[24] G. Grosso, G. Nardin, F. Morier-Genoud, Y. Léger, and B. Deveaud-Plédran, Phys. Rev. Lett. **107**, 245301 (2011).
[25] A. Amo, S. Pigeon, D. Sanvitto, V. G. Sala, R. Hivet, I. Carusotto, F. Pisanello, G. Leménager, R. Houdré, E. Giacobino, C. Ciuti, and A. Bramati, Science **332**, 1167 (2011).
[26] C. Schneider, K. Winkler, M. D. Fraser, M. Kamp, Y. Yamamoto, E. A. Ostrovskaya, and S. Höfling, Rep. Prog. Phys. **80**, 016503 (2017).
[27] T. J. Alexander, E. A. Ostrovskaya, and Y. S. Kivshar, Phys. Rev. Lett. **96**, 040401 (2006).
[28] J. Wang, J. Yang, T. J. Alexander, and Y. S. Kivshar, Phys. Rev. A **79**, 043610 (2009).
[29] T. Anker, M. Albiez, R. Gati, S. Hunsmann, B. Eiermann, A. Trombettoni, and M. K. Oberthaler, Phys. Rev. Lett. **94**, 020403 (2005).
[30] F. H. Bennet, T. J. Alexander, F. Haslinger, A. Mitchell, D. N. Neshev, and Y. S. Kivshar, Phys. Rev. Lett. **106**, 093901 (2011).
[31] C. Bersch, G. Onishchukov, and U. Peschel, Phys. Rev. Lett. **109**, 093903 (2012).
[32] See Supplemental Material at http://link.aps.org/supplemental/10.1103/PhysRevLett.123.113901 for additional experimental data and numerical simulations, which includes Ref. [33].
[33] T. Alexander and Y. Kivshar, Appl. Phys. B **82**, 203 (2006).
[34] I. Carusotto and C. Ciuti, Phys. Rev. Lett. **93**, 166401 (2004).
[35] A. Baas, J. P. Karr, H. Eleuch, and E. Giacobino, Phys. Rev. A **69**, 023809 (2004).
[36] A. Amo, T. C. H. Liew, C. Adrados, R. Houdré, E. Giacobino, A. V. Kavokin, and A. Bramati, Nat. Photonics **4**, 361 (2010).
[37] E. Togan, H.-T. Lim, S. Faelt, W. Wegscheider, and A. Imamoglu, Phys. Rev. Lett. **121**, 227402 (2018).
[38] I. Rosenberg, D. Liran, Y. Mazuz-Harpaz, K. West, L. Pfeiffer, and R. Rapaport, Sci. Adv. **4**, eaat8880 (2018).
[39] S. I. Tsintzos, A. Tzimis, G. Stavrinidis, A. Trifonov, Z. Hatzopoulos, J. J. Baumberg, H. Ohadi, and P. G. Savvidis, Phys. Rev. Lett. **121**, 037401 (2018).
[40] P. Knüppel, S. Ravets, M. Kroner, S. Fält, W. Wegscheider, and A. Imamoglu, arXiv:1903.09256.
[41] C. Wu, D. Bergman, L. Balents, and S. Das Sarma, Phys. Rev. Lett. **99**, 070401 (2007).
[42] K. Sun, Z. Gu, H. Katsura, and S. Das Sarma, Phys. Rev. Lett. **106**, 236803 (2011).
[43] T. Neupert, L. Santos, C. Chamon, and C. Mudry, Phys. Rev. Lett. **106**, 236804 (2011).
[44] L. W. Clark, N. Schine, C. Baum, N. Jia, and J. Simon, arXiv:1907.05872.